**Cell Reports, Volume *24***

## Supplemental Information

# A Genetically Encoded Biosensor Strategy for Quantifying Non-muscle Myosin II Phosphorylation Dynamics in Living Cells and Organisms

**Michele L. Markwardt, Nicole E. Snell, Min Guo, Yicong Wu, Ryan Christensen, Huafeng Liu, Hari Shroff, and M.A. Rizzo**

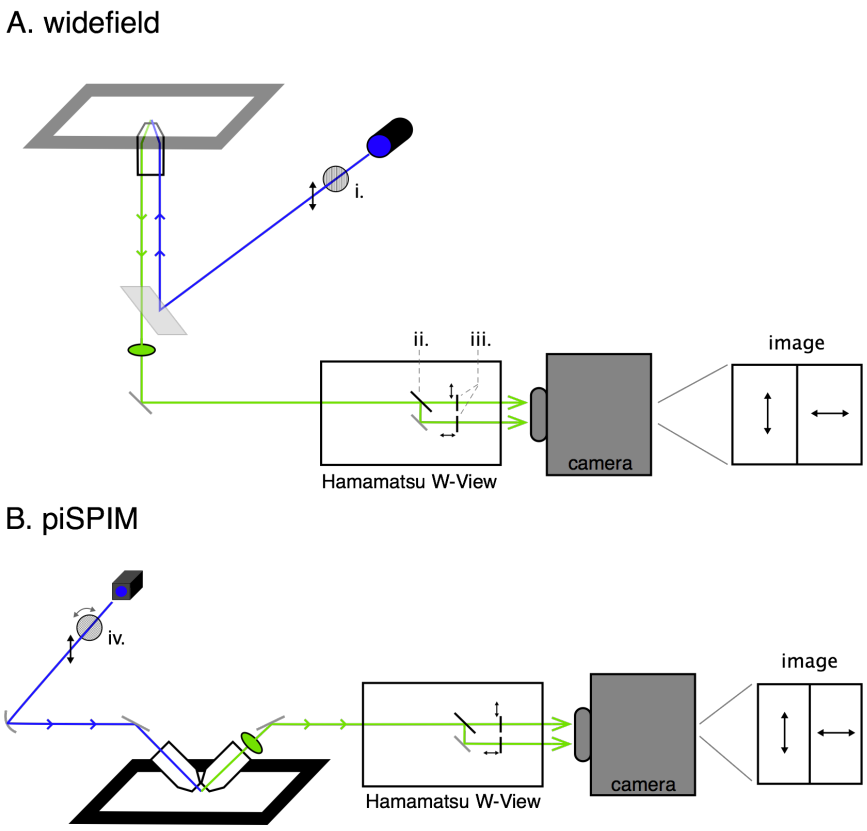


**Figure S1. Optical configurations for fluorescence polarization microscopy**. **Related to the STAR Methods**. **A**. A widefield sample configuration. LED illumination is filtered by a plane polarizer before deflection to the objective lens by a standard fluorescence filter cube. The emitted light is filtered for color first by the filter cube. *P* and *S* polarizations are separated by an image splitting device and collected simultaneously using a single camera. Commercial polarization splitting configurations are available from Optical insights (Dual-View) or Cairn (Opto-Split). Alternatively, the W-view Gemini from Hamamatsu can be custom fitted with polarization splitting optics. Optics i-iii are Versalight unmounted wired grid polarizers (Meadowlark Optics). **B.** For piSPIM imaging, laser polarization is controlled using a rotatable λ/2 waveplate (iv, Thorlabs) inserted into the beam path. A W-view fitted with the polarization optics depicted in **A** (ii, iii) was used to separate emitted *P* and *S* polarizations.

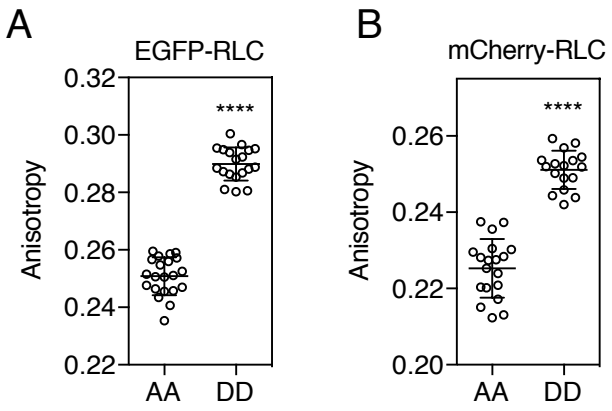


**Figure S2. EGFP and mCherry RLC biosensors. Related to the Figure 1**. Alternate RLC biosensors were constructed using EGFP (**A**) and mCherry (**B**). RLC phosphorylation sites (Ser19, and Thr18 (Ikebe et al., 1986)) were mutated to alanines (AA) to prevent phosphorylation or aspartates (DD) to mimic RLC phosphorylation. Anisotropies were calculated from widefield (20× magnification, 0.8 NA lens) images of cells expressing the indicated constructs, as described in the methods. T-tests were used to determine statistical significance for EGFP-RLC (****, $p < 0.0001$; AA, n = 21; DD, n=19 biological replicates) and mCherry-RLC (****, $p < 0.0001$; AA, n = 19; DD, n=17 biological replicates). Bars indicate mean ± SD.

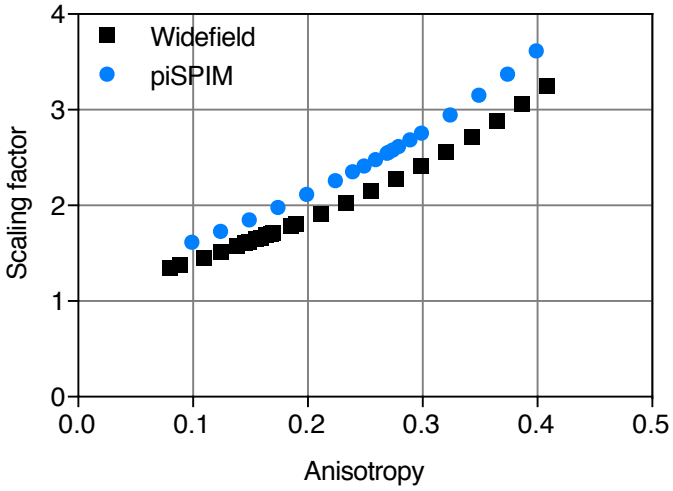


**Figure S3. Scaling factor calculations. Related to the Figures 1 and 5**. Theoretical $P$ and $S$ values were used to calculate fluorescence anisotropies and scaling factors $P/(S \times g)$ for normalized subtraction. Related to the Figures 1 and 5. Calculations are shown for the two $g$ factors used in this study ($g$ = 1.05 for widefield; $g$ = 1.2 for piSPIM).

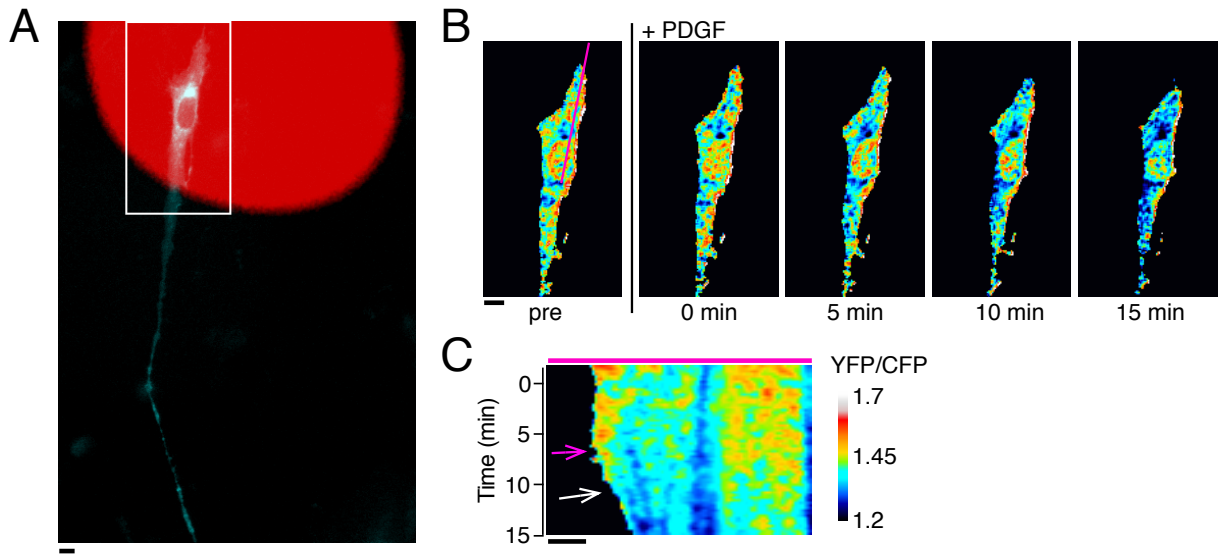


**Figure S4. Local changes in RhoA activity during retraction. Related to the Figure 4**. RhoA activity in response to local application of PDGF was assessed in REF52 fibroblasts expressing a FRET biosensor. **A.** Application of PDGF (10 ng/ml) with a microfluidic pipette was marked using rhodamine (red). Cyan fluorescence from the REF52 cell is overlaid with the rhodamine image. **B.** FRET ratio images were generated for the REF52 cell over time, showing a PDGF-induced retraction. The pink line in panel 1 was used to create a kymograph (**C**). Retraction proceeds slowly at the beginning (pink arrow). Accelerated movement (white arrow) is associated with a decrease in the YFP/CFP FRET ratio, indicating deactivation of RhoA. Scale bars are 10 microns, and the FRET ratios are indicated by pseudocolor as shown. Images are representative of 6 biological replicates.

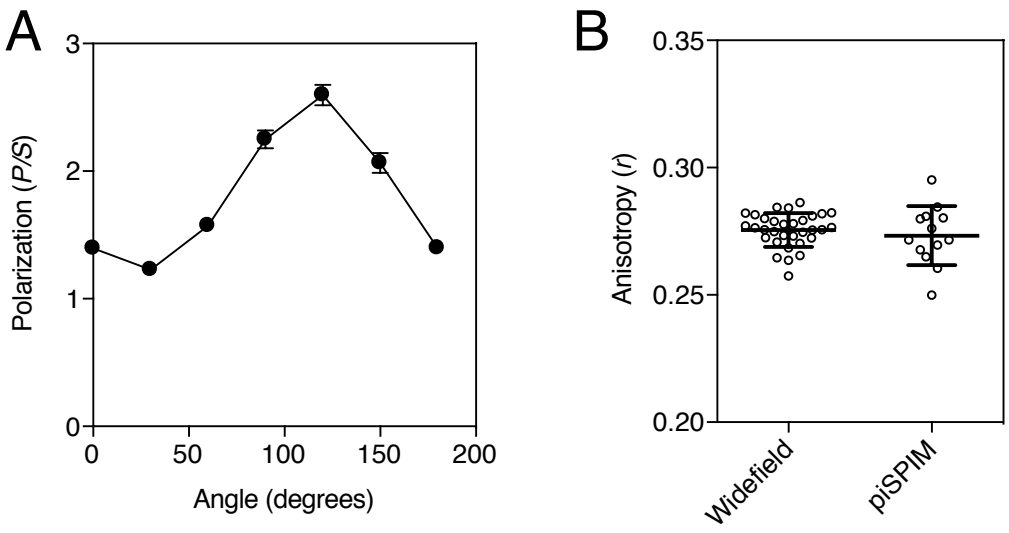


**Figure S5. GFP polarization measurements using piSPIM. Related to the Figures 5 and 6**.

**A.** A half-wave plate was inserted in the beam path and rotated at regular increments to optimize the laser polarization for piSPIM. GFP-labeled beads were imaged at the indicated angles and the *P*/*S* polarization ratio computed. Bars indicate mean ± SD. (n=13 biological replicates per point, each angle is a technical replicate) **B.** The measured GFP-bead anisotropy in piSPIM agreed well with bead measurements taken by widefield microscopy. Bars indicate mean ± SD. (n= 32 biological replicates for widefield; n=13 biological replicates for piSPIM; mean *r* values are not statistically different (t-test, $p > 0.05$)).

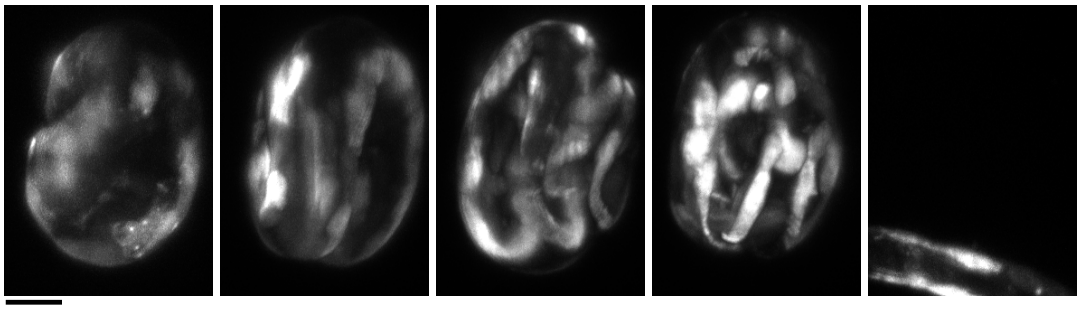

| stage | comma | two-fold | three-fold | cuticle synthesis | hatched |
|---|---|---|---|---|---|
| imaging time | 20 min | 85 min | 140 min | 280 min | 435 min |
| embryo time | 430 min | 490 min | 550 min | 690 min | 840 min |

**Figure S6. Embryo morphology during piSPIM imaging. Related to the Figure 5.** Maximum intensity projections are shown for z-stacks collected by piSPIM imaging of GFP-MLC-4. Developmental stage, time since the onset of imaging, and embryonic time defined from fertilization are indicated. Scale bar = 10 μm

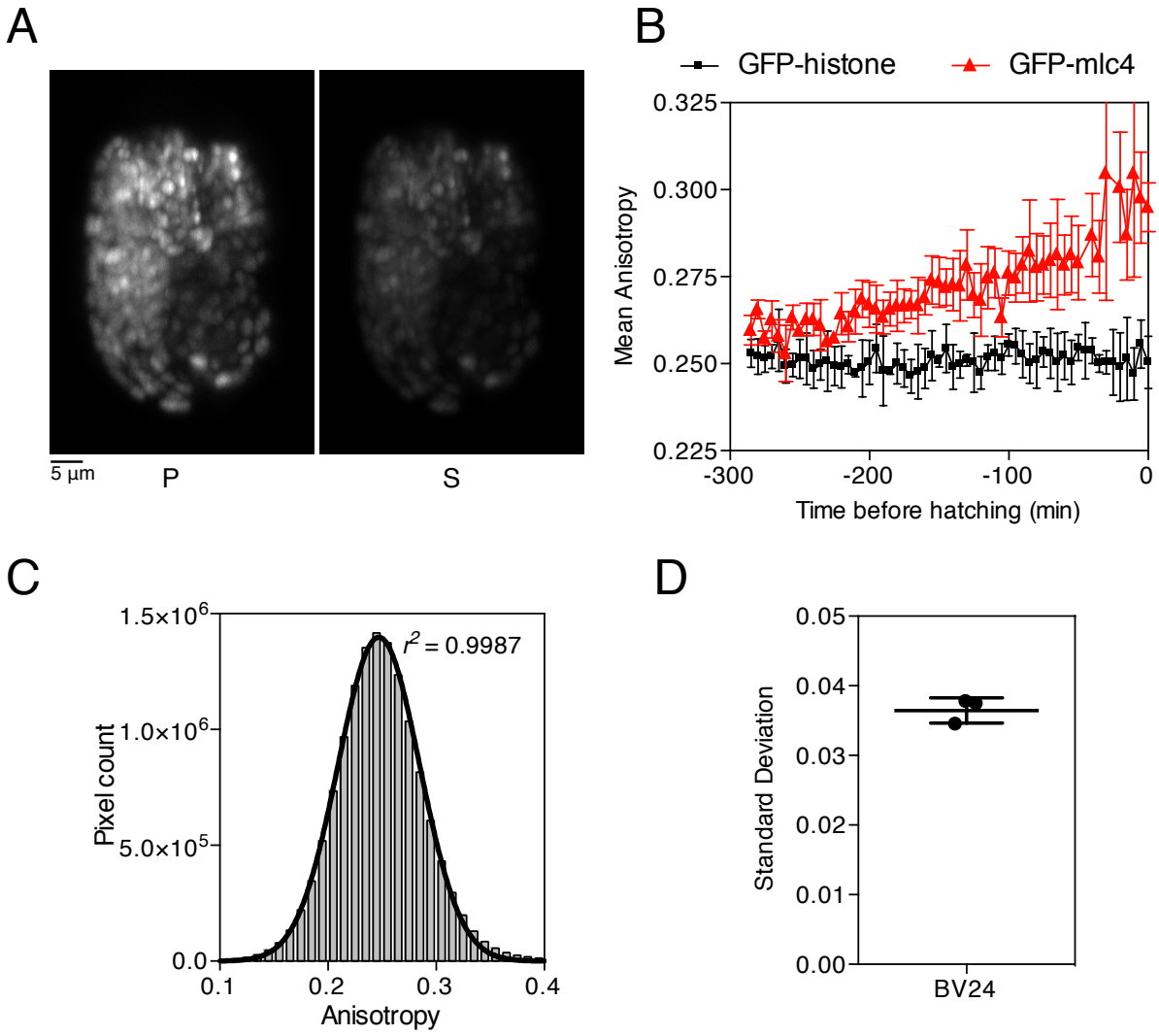


**Figure S7. piSPIM imaging of GFP-tagged histone in *C. elegans*. Related to Figure 6. A.** BV24 embryos expressing a GFP-histone were imaged using piSPIM from the mid-elongation phase until hatching. Maximum intensity projections of an embryo 200 min before hatching are shown for both *P* and *S* polarizations, scale bar = 5 µm. **B.** The average anisotropy for individual time points was calculated for three biological replicates (bars = SEM). **C.** The distribution of pixel anisotropies for an entire data set is shown. The data was fit to a one component Gaussian fit. **D.** Measured standard deviations from three biological replicates were averaged and used for fitting the GFP-MLC-4 anisotropies. Bars indicate mean ± SD.